

---

This is an electronic reprint of the original article.  
This reprint may differ from the original in pagination and typographic detail.

Guo, Tianyu; Wan, Zhangmin; Li, Dagang; Song, Junlong; Rojas, Orlando J.; Jin, Yongcan  
**Intermolecular self-assembly of dopamine-conjugated carboxymethylcellulose and carbon nanotubes toward supertough filaments and multifunctional wearables**

*Published in:*  
Chemical Engineering Journal

*DOI:*  
[10.1016/j.cej.2021.128981](https://doi.org/10.1016/j.cej.2021.128981)

Published: 15/07/2021

*Document Version*  
Publisher's PDF, also known as Version of record

*Published under the following license:*  
CC BY

*Please cite the original version:*  
Guo, T., Wan, Z., Li, D., Song, J., Rojas, O. J., & Jin, Y. (2021). Intermolecular self-assembly of dopamine-conjugated carboxymethylcellulose and carbon nanotubes toward supertough filaments and multifunctional wearables. *Chemical Engineering Journal*, 416, Article 128981. <https://doi.org/10.1016/j.cej.2021.128981>

---

This material is protected by copyright and other intellectual property rights, and duplication or sale of all or part of any of the repository collections is not permitted, except that material may be duplicated by you for your research use or educational purposes in electronic or print form. You must obtain permission for any other use. Electronic or print copies may not be offered, whether for sale or otherwise to anyone who is not an authorised user.



# Intermolecular self-assembly of dopamine-conjugated carboxymethylcellulose and carbon nanotubes toward supertough filaments and multifunctional wearables

Tianyu Guo<sup>a,b</sup>, Zhangmin Wan<sup>c</sup>, Dagang Li<sup>c</sup>, Junlong Song<sup>a</sup>, Orlando J. Rojas<sup>b,d,\*</sup>, Yongcan Jin<sup>a,\*</sup>

<sup>a</sup> Jiangsu Co-Innovation Center of Efficient Processing and Utilization of Forest Resources, and Jiangsu Provincial Key Lab of Pulp and Paper Science and Technology, Nanjing Forestry University, Nanjing 210037, PR China

<sup>b</sup> Bioproducts Institute, Departments of Chemical and Biological Engineering, Chemistry and Wood Science, The University of British Columbia, 2360 East Mall, Vancouver, BC V6T 1Z3, Canada

<sup>c</sup> College of Material Science and Engineering, Nanjing Forestry University, Nanjing 210037, PR China

<sup>d</sup> Department of Bioproducts and Biosystems, School of Chemical Engineering, Aalto University, P.O. Box 16300, FI-00076 Aalto, Espoo, Finland

## ARTICLE INFO

### Keywords:

Intermolecular self-assembly  
Multifunctional filaments  
Wearables  
Sensors  
Electrothermal heating  
Nanocomposites

## ABSTRACT

The utilization of smart textiles, mainly in the form of yarns and wovens, requires high structural toughness and flexibility. To this end, we introduce a strategy based on the intermolecular self-assembly of dopamine-conjugated carboxymethyl cellulose (DA-CMC) with carbon nanotubes (CNT). Upon coagulation in a non-solvent, the DA-CMC/CNT suspensions readily form composite filaments by the effects of hydrogen bonding, H- $\pi$ , anion- $\pi$ , and  $\pi$ - $\pi$  interactions, as demonstrated by molecular dynamic simulation. The DA-CMC/CNT filaments display super-toughness ( $\sim 76.2 \text{ MJ m}^{-3}$ ), extensibility (strain to failure of  $\sim 14.8\%$  at 90% RH, twice that of dopamine-free analogous systems) and high electrical conductivity. Moreover, the composite filaments form conductive networks that effectively support bending, strain and compression in air or fluid media. As such, they are suitable for application in wearables devices designed for sensing and electrothermal heating. Our proposed, scalable synthesis of multifunctional filaments opens new opportunities given their electroactivity and suitability for human interfacing.

## 1. Introduction

Multifunctional electronics have been widely applied for human-computer interaction [1] and in medical implants [2] and thermoelectrics [3]. In these areas, conductive materials, usually in the form of yarns, strands and wovens [4–7], have gained great attention mainly due to their lightweight and suitability for implementation in the “Internet of Things” [8]. Previous studies focusing on multifunctional wearable electronics revealed that stability of energy interconversion [9–11] together with a high mechanical performance [12], for example under periodic mechanical motion, are key aspects for the success of related applications. Because their excellent mechanical properties, electrical and thermal conductivity, semiconductor materials, such as carbon nanotubes (CNTs) and graphene, have been the materials of choice for the fabrication of wearable electronics [13–15]. However,

transferring their outstanding performance, from the atomic scales to the macroscales, depends on flawless structural designs and interface connectivity, which can be limited in the case of macroscopic materials built with CNTs or graphene, which tend to be brittle [16]. Indeed, they endow systems with a very high strength and Young’s modulus but with relatively low fracture toughness [17,18].

To address the above limitations, intermolecular assembly has been considered as an efficient strategy to organize nanoscale building blocks into macroscopic materials [19,20]. We utilized wet-spinning to fabricate highly tough ( $\sim 19 \text{ MJ m}^{-3}$ ) filaments of CNT and cellulose nanofibrils (CNF) [21] while ionic crosslinking and intermolecular bonding were effective for the synthesis of graphene filaments with similar performance ( $18.7 \text{ MJ m}^{-3}$ ) [22]. In related processes, hydrogels exhibit a high toughness, given the capability for stretching and slippage of molecular chains, involving multiscale interactions [23]; thus, they can be

\* Corresponding authors.

E-mail addresses: [orlando.rojas@ubc.ca](mailto:orlando.rojas@ubc.ca) (O.J. Rojas), [jinyongcan@njfu.edu.cn](mailto:jinyongcan@njfu.edu.cn) (Y. Jin).

<https://doi.org/10.1016/j.cej.2021.128981>

Received 28 October 2020; Received in revised form 23 December 2020; Accepted 10 February 2021

Available online 16 February 2021

1385-8947/© 2021 The Authors. Published by Elsevier B.V. This is an open access article under the CC BY license (<http://creativecommons.org/licenses/by/4.0/>).

considered as candidates for multifunctional devices [24,25]. Unfortunately, hydrogels are rather sensitive to water, leading to brittle or fragile systems once water is removed, for example, during Joule heating or upon evaporation at body temperatures. This prevents practical deployment of hydrogels in such applications [26]. Thus, a serious challenge still remains to meet the requirements of wearable electronics, namely, the synthesis of macroscopic materials with both high toughness and durability when exposed to typical conditions.

Inspired by mussel adhesive proteins, we reported on a biomimetic composite with dopamine (DA)-conjugated CMC (DA-CMC), which was subsequently assembled with montmorillonite. The DA-grafted CMC maintained the interfacial strength of the composite, even at high humidity (162 MPa, with an elastic modulus of 8.7 GPa at 90% RH) [27]. Dopamine (DA)-conjugated CMC (DA-CMC) was found to form a robust framework through secondary bonding (anion- $\pi$  [28],  $\pi$ - $\pi$  [29], and van der Waals [30,31] interactions as well as hydrogen bonding [32]), wrapping around CNTs to toughen their interfaces.

Herein, we propose a self-assembly strategy involving aqueous suspensions of DA-CMC and CNT that can be wet-spun in a nonsolvent (ethanol) to yield water-resistant and supertough filaments (DA-CMC/CNT). We demonstrate a continuous self-assembly strategy that leads to filaments with oriented hydrogen bonding as well as strong interfibril interactions. As a result, ultra-flexible and conductive DA-CMC/CNT filaments were used for their electrothermal activity. We demonstrate corresponding wearable materials that display responsiveness to multiple external stimuli (humidity, mechanical and electrical), endowing rapid electrothermal and electromechanical sensing, with great promise for application in next-generation wearables.

## 2. Experimental section

### 2.1. Materials

Carboxymethylcellulose (CMC, sodium form,  $M_w = 700,000 \text{ g mol}^{-1}$ , degree of substitution,  $DS = 0.9$ , Aldrich, USA), dopamine (DA, 98%,  $189.6 \text{ g mol}^{-1}$ ), N-hydroxysuccinimide (NHS), 1-(3-dimethylamino-propyl)-3-ethylcarbodiimide hydrochloride (EDC) were all purchased from Sigma Aldrich (Milwaukee, USA). Single-walled carbon nanotubes (CNT, XFS 19, diameter 1–2 nm, length 1–3  $\mu\text{m}$ ) were obtained from XFNANO Inc., China. Other chemicals were purchased from Nanjing Chemical Reagent Co., Ltd. (Nanjing, China).

### 2.2. Synthesis of DA-CMC and DA-CMC/CNT

DA-grafted CMC (DA-CMC) was prepared via EDC/NHS coupling, as described earlier [27]. (FTIR spectra indicated the successful conjugation between CMC and DA in Figure S18). CNT was added to a concentrated DA-CMC solution at a given loading (from 5 to 20 wt%) under ultrasonication (20 min). Following, DA-CMC/CNT dispersions were prepared and used to synthesize the filaments. CMC/CNT filaments (with no DA grafted to CMC) were also produced as a reference. Herein, the systems are referred to as DA-CMC/CNT-5, DA-CMC/CNT-10, DA-CMC/CNT-20, CMC/CNT-5, CMC/CNT-10, and CMC/CNT-20, where 5, 10, and 20 indicating the mass ratio of CNT with respect to the total weight.

### 2.3. Preparation of filaments by wet-spinning

The DA-CMC/CNT and CMC/CNT suspensions were spun in an ethanolic rotating bath (water:ethanol volume ratio of 3:1) using a needle set on a syringe (5 mL) driven by a pump operated at 4.2 mL/min. The wet-spun DA-CMC/CNT gel microfiber was towed out from the coagulation bath after dipping for 20 min, under stretching. After plasticizing and stretching, the gel filaments were dried at room temperature under a small tensile load.

### 2.4. Chemical characterization

UV-vis and NIR absorption spectra were recorded with a Lambda 950 spectrophotometer (PerkinElmer, USA) at a scan rate of 600 nm/min using 10 mm path length quartz cuvettes, using the signal from water as the baseline. The specific absorption for CNTs dispersed in DA-CMC suspensions was calculated on the basis of Beer-Lambert law [33].

### 2.5. Shear viscosity

Rheology measurements were carried out on DA-CMC/CNT suspensions using a rheometer (MAR S60, Thermo Fisher Scientific, Germany) operated at room temperature with a 25-mm diameter parallel plate setup with a truncation gap of 0.5 mm. The shear rate was ramped from 0.1 to 1000  $\text{s}^{-1}$  and the Carreau viscosity model was used to determine the effective viscosity,  $\eta_{\text{eff}}$ :

$$\eta_{\text{eff}}(\dot{\gamma}) = \eta_{\text{inf}} + (\eta_0 - \eta_{\text{inf}})[1 + (\tau\dot{\gamma})^2]^{(n-1)/2} \quad (1)$$

where  $\eta_{\text{eff}}$  is the viscosity,  $\dot{\gamma}$  is the shear rate,  $\eta_{\text{inf}}$  and  $\eta_0$  are the viscosities at infinite shear and zero shear rate, respectively.  $\tau$  is the relaxation time and  $n$  is the power index. The parameters from the best fits are listed in Table S2.

### 2.6. Filament morphology and strength

A circular cross section was assumed for the filaments and the diameters were measured with an optical microscope (BX51, OLYMPUS, Japan). The average of 20 measurements was determined from samples that were randomly selected (Figure S1). The linear density of the filaments was calculated by dividing the mass of the filament (microbalance) with a given length ( $\sim 3 \text{ m}$ ) (Table S1). The fiber ends were glued on paper (Figure S2), and the whole assembly was mounted on the tensile test instrument and clamped between the grips. The filaments were held by the grips on both ends, while the vertical part of the paper strip was cut from the center. The span length was 9–12 mm, and the measurements were carried out at a crosshead speed of 0.5  $\text{mm min}^{-1}$ . Scanning electron microscopy was performed with a JSM-6400 SEM instrument (JEOL, Japan) to observe the surface and cross-section of the filaments at an accelerating voltage of 10 kV. The mechanical properties were measured in the tensile mode using a CMT4202 versatile testing machine (SANS, China) with a 5 N load cell. Filaments were conditioned at room temperature (23  $^\circ\text{C}$ ) and 50 or 90% RH for at least 48 h prior to testing.

### 2.7. Molecular dynamics simulation (MDS)

MDS was performed using Gromacs package [34], version 2018.3, and OPLS all-atom force field [35] to mimic the materials used in this investigation. The CNT was built as an index of 0.6 nm width and 5 nm length by Nanotube Modeler [36]. The DA-CMC and CNT (mass ratio of 9:1) were placed in a cubic box ( $15 \times 15 \times 15 \text{ nm}^3$ ) implemented in Gromacs. Firstly, the simulations were run in NVE ensemble, where the temperature was kept constant at 300 K using a V-rescale method for 10 ns. The RMSD of the DA-CMC and CNTs was analyzed by using gmx rms tool. Then, the systems were optimized by energy minimization using the steepest descent method for 1 ns. After the equilibration, constant velocity steered molecular dynamics (SMD) was used to calculate the mechanical properties of the composites. The force was calculated during SMD by using the following equations:

$$F = -\nabla U \quad (2)$$

$$U = \frac{1}{2} k [vt - (r - r_0) \cdot n]^2 \quad (3)$$

where  $\nabla U$  is the potential energy gradient,  $k$  is the spring force constant,

$v$  is the velocity,  $t$  is the current time,  $r$  is the real-time vector position,  $r_0$  is the starting vector position, and  $n$  is the vector direction in which the dummy atom is pulled. After SMD, the strength of the composites was obtained by dividing the force by the fracture cross section. Hydrogen bonding was studied by using the gmh hydrogen tool. Only the hydrogen bonds formed by hydroxyl and carboxyl groups were considered. A donor–acceptor distance of 0.35 nm and an angle cutoff of  $30^\circ$  were used as criteria for hydrogen bond determination. The energy of non-bonded interactions was analyzed by using the gmh energy tool. The structure optimization of DA-CMC is based on density function theory (DFT) method B3LYP [37] in conjunction with def2-TZVP basis set [38]. The structure optimization of CNT is based on CAM-B3LYP method [39] in conjunction with def2-TZVP basis set [38]. To explore the non-bonded interaction between DA-CMC and CNT, the single point energy of composite structure is calculated by GFN-xTB method [40].

## 2.8. Conductivity

The electrical volume resistivities of the filaments were measured with a bench-type multimeter (UT-803, UNI-T, China) and recorded simultaneously by a software (UT-803 Interface Program\_Ver: 0.1). Prior testing, the samples (2-cm in length), were conditioned at room temperature and 50% RH, for at least 2 days. The composite filaments and conductive copper wires were connected by using silver paste. The electrical conductivity of the filaments was calculated according to the resistivity formula (Table S3). To investigate the water sensitivity of the filaments, the resistance values were collected by a computer-controlled liquid sensing setup with a sampling rate of 1 s and measured by

immersion and drying. Both processes were carried out in air (50% RH) at room temperature. Before testing, any liquid drops remaining on the test fixture were carefully wiped off using a tissue.

## 2.9. Thermal responsiveness

Infrared thermal imaging was carried out to detect in real time the temperature changes (infrared thermal camera ThermoVision A20, FLIR, USA). The samples used for resistance testing were energized by a dc power supply (PS-1502D<sup>+</sup>, BEST, China). The electro-thermal performance was accessed by using a hand glove that was sewn with 10 filaments. The thermal images and temperature of the system were monitored by an IR camera (FOTRIC 226, USA).

## 2.10. Sensor fabrication

A filament-based flexible sensor was constructed by twisting five DA-CMC/CNT filaments and linked with two metallic electrodes. The electrical signals of the samples were recorded by fixing them between two boards under dynamically applied strains. Incremental weights were placed on the strain sensors to record changes in electrical resistance at room temperature by using a benchtop multimeter. The strain sensor was applied to human skin to detect motions in real-time.

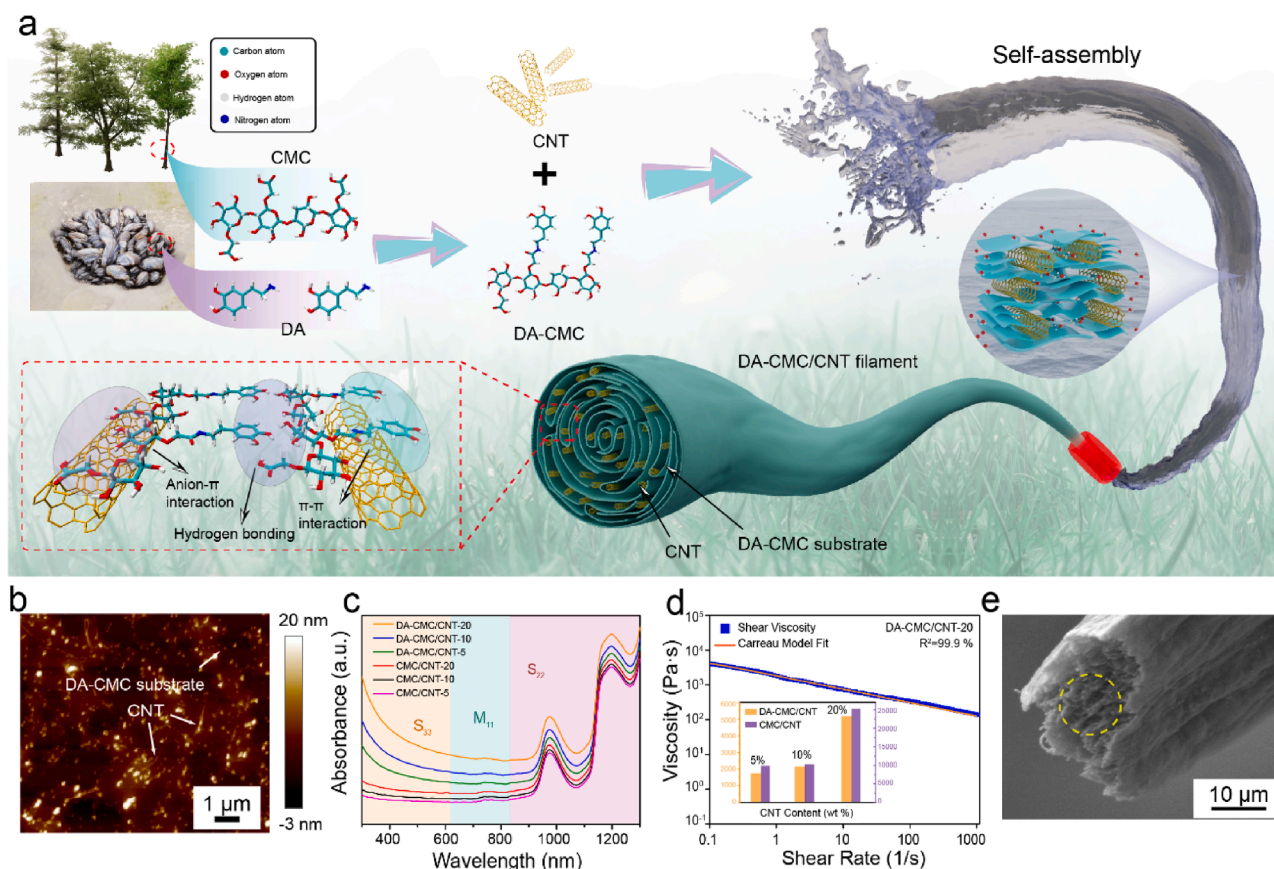


**Fig. 1.** Intermolecular assembly of DA-CMC and CNT. (a) Schematic illustration of the synthesis of self-assembled filaments comprising DA-CMC and CNT. (b) AFM image of DA-CMC/CNT supported on mica. (c) UV-vis-NIR absorbance for CMC/CNT and DA-CMC/CNT suspensions with different CNT loading, as indicated by the numerals used in the labels. (d) Shear viscosity measured for DA-CMC/CNT dispersion, showing a shear thinning behavior. Inset: Viscosity of dispersions with different CNT content (5, 10 and 20%). (e) Cross-sectional SEM image of a DA-CMC/CNT filament. The yellow dashed circle highlight an area indicating DA-CMC wrapping around CNTs. (For interpretation of the references to colour in this figure legend, the reader is referred to the web version of this article.)

### 3. Results and discussion

#### 3.1. Preparation and characterization of the DA-CMC/CNT dispersion

DA-CMC was synthesized following our earlier work [21,27], and used here to disperse CNT under ultrasonication and mechanical stirring (Fig. 1a). CNT tends to aggregate in water, due to strong interparticle interactions [41]; however, this is not the case in the presence of DA-CMC, given the strong interactions between these components (see AFM image in Fig. 1b). UV-vis-NIR absorbance spectra for DA-CMC/CNT and CMC/CNT at different CNT content are shown in Fig. 1c (Note: the nomenclature refers to CNT loading, given as % weight with respect to DA-CMC, from 5 to 20 wt%). The colloidal stability of the systems was confirmed by the narrow, blue-shifted peaks in the absorbance spectra [42]. Except for slight variations, no significant differences were noted in the spectra acquired from the different samples (Fig. 1c). The optical density at 500 nm of CNT in CMC as well as DA-CMC dispersions, measured at different concentrations, indicated a linear correlation with absorbance (linear-least-squares fit, Figure S3), indicating well-dispersed CNTs in DA-CMC. TEM was used to access the morphology of DA-CMC/CNT (Figure S4), suggesting that CNT existed as single-stranded structures with a uniform diameter ( $\sim 3$  nm height). The CMC/CNT and DA-CMC/CNT dispersions were colloidally stable after storage for at least three months, with no evidence of phase separation.

The apparent viscosity of the dispersions increased with CNT loading (Fig. 1d) and they were shown to be shear-thinning (fitting the Carreau model, Figure S5). To further explore the mechanism of wet spinning and to simulate the flow of the dispersions in the nozzle, we utilized finite element modelling (FEM) (Figure S6). The results indicate that the DA-grafted CMC decreased the viscosity of the dispersion, leading to a velocity reduction at the nozzle (Figure S7). This effect extensively reduced the chances of nozzle blockage, facilitating the extrusion process during spinning.

#### 3.2. Mechanical properties of DA-CMC/CNT filaments

Given the synergetic interactions between DA-CMC and CNTs, the wet-spun filaments exhibited excellent toughness. Fig. 2a,b show typical tensile stress-strain curves of DA-CMC/CNT-10 and CMC/CNT-10 filaments measured at 50% and 90% RH, respectively. The DA-CMC/CNT-10 filaments exhibited a tensile strength of 457 MPa and toughness of  $76 \text{ MJ m}^{-3}$ . In comparison, the corresponding values for CMC/CNT-10 filaments were 294 MPa and  $63 \text{ MJ m}^{-3}$ . The increased toughness in filaments formed with dopamine-coupled CMC is attributed to the reduced structural defects in the macrofibers, as well as the strong secondary interactions between DA-CMC and CNT, which ensure a high cohesion between the building blocks. Besides, the strain at failure obtained from the stress-strain profiles showed optimal performance in the system with CNT associated with DA-CMC (Fig. 2c): the failure strain of DA-CMC/CNT-10 filaments ( $\sim 15\%$  at 90% RH) was twice that in the absence of dopamine (CMC/CNT-10 sample). The stress-strain curves for CMC/CNT and DA-CMC/CNT filaments with 5% and 20% CNT and under different humidity are shown in Figure S8. All the results indicate that the presence of dopamine significantly increased the interfacial adhesion between the building blocks, especially under humid environments. This is in line with the fact that catecholic amino acids, a major component in the mussel's foot proteins [43], are effective in the development of underwater adhesion via hydrogen bonding, pi-pi aromatic interaction, cation-pi interaction, metal-catechol coordination, and electrostatic interactions [44,45]. Finally, the fractured surface after tensile failure (SEM image in Fig. 1e) showed that the CNT initially embedded in the DA-CMC matrix was pulled out in the direction of deformation. This indicated an extensive stress transfer and confirmed ordered packing. In Fig. 2f, a knotted filament is shown to illustrate the excellent toughness and knittability.

Our DA-CMC/CNT filaments exhibited a toughness that is much higher than that measured in synthetic counterparts as well as filaments produced from HDPE, PP, Viscose, and Lyocell (Fig. 2d,e, measured at

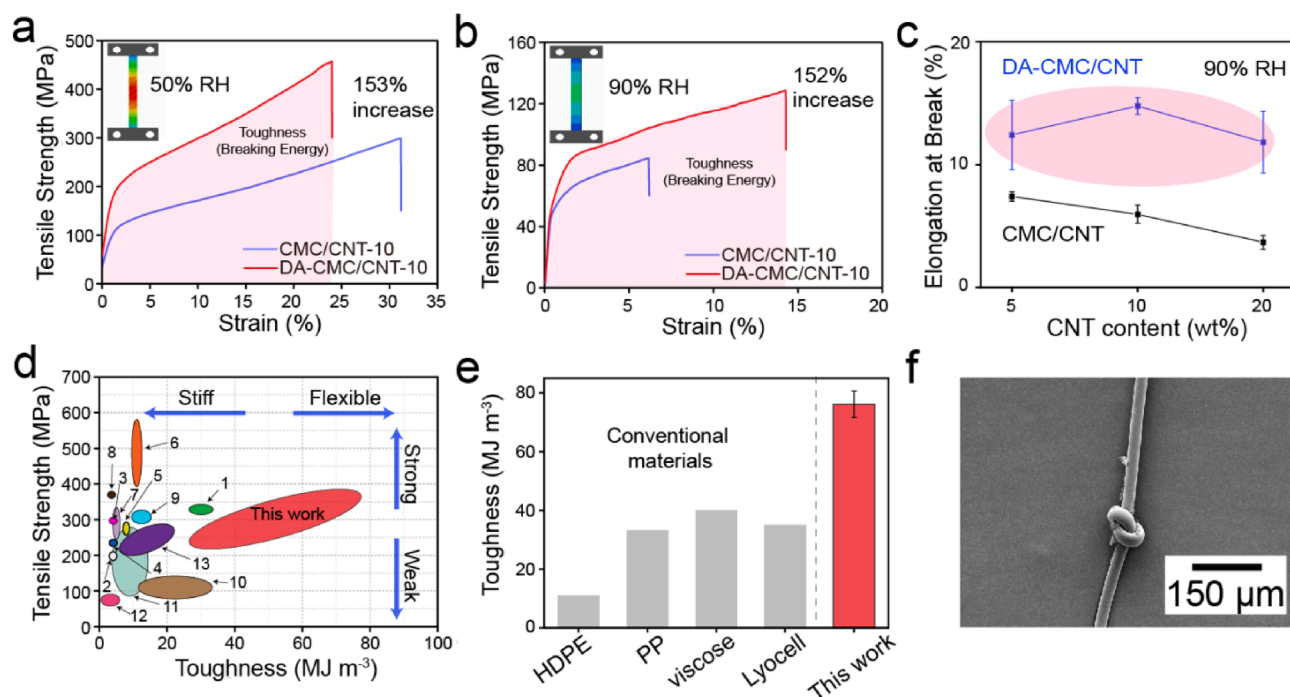


**Fig. 2.** Supertough filaments produced from DA-CMC/CNT. (a, b) Stress-strain profiles for CMC/CNT and DA-CMC/CNT at 50% and 90% RH. Inset: the stress map for filaments during mechanical testing. (c) Failure strain of DA-CMC-CNT filaments measured at 50% and 90% RH. (d) A map of tensile strength versus toughness of filaments containing cellulose (nanocelluloses or cellulose derivatives) together with carbon nanomaterials reported in the literature (the numerals refer to references given in the Supporting Information, Table S4). (e) Toughness of DA-CMC/CNT filaments compared to those produced from HDPE, PP, Viscose, and Lyocell (see details as Supporting Information, Table S4 and references therein). (f) SEM image of a knotted DA-CMC/CNT filament.

RH < 50%). Some nanocellulose-based filaments exhibit a high strength due to stiff and crystalline cellulose [46]. Even though abundant hydrogen bonding contributes to toughness, the accumulative internal stress promotes rapid fracture between building blocks, thus, reducing the strain at failure. Here, the super-toughness observed for DA-CMC/CNT filaments is hypothesized to result from reduced structural defects in the macrofibers and the facile formation and reformation of non-bonding interactions among molecular chains. These features contribute to an effective cohesion between building blocks undergoing stretching and slippage under load [32]. Finally, despite the reduction in toughness under high humidity, the DA-CMC/CNT filaments satisfy the demands under such conditions (compare Fig. 2a and 2b).[47]

### 3.3. Molecular dynamic simulation of the DA-CMC/CNT interaction

Theoretical studies predict CNT to act as a reinforcement phase

(mechanical strength, electrical conductivity) in polymer composites. However, the metrics of the properties reported in such studies are rather scattered because of the nature of the interfacial separation and sliding between the components. Additionally, the weak bonding formed between CNTs and polymer matrices have not been compared systematically.[48] Nevertheless, the secondary bonding between CNT and DA-CMC or CMC can be considered. Fig. 3a illustrates the multiscale interactions between DA-CMC and CNTs in aqueous media, and includes the Electrostatic Potential (ESP) of DA-CMC and the pi electron orbital of catechol (for details, see Figures S9 and S10 in Supporting Information). On the surface of DA-CMC molecular chains, the lowest ESP is  $-0.067$  atomic units (a.u.), while the highest ESP is  $0.11$  a.u. After 5 ns, the DA-CMC starts to wrap around CNT, mainly through anion-pi interactions and H-pi interactions, which can be demonstrated by the inserted contour line map of Laplacian electron density ( $\nabla^2\rho$ )[49]. Also, the catechol group in DA-CMC generates pi-pi interactions with CNTs at 30 ns.

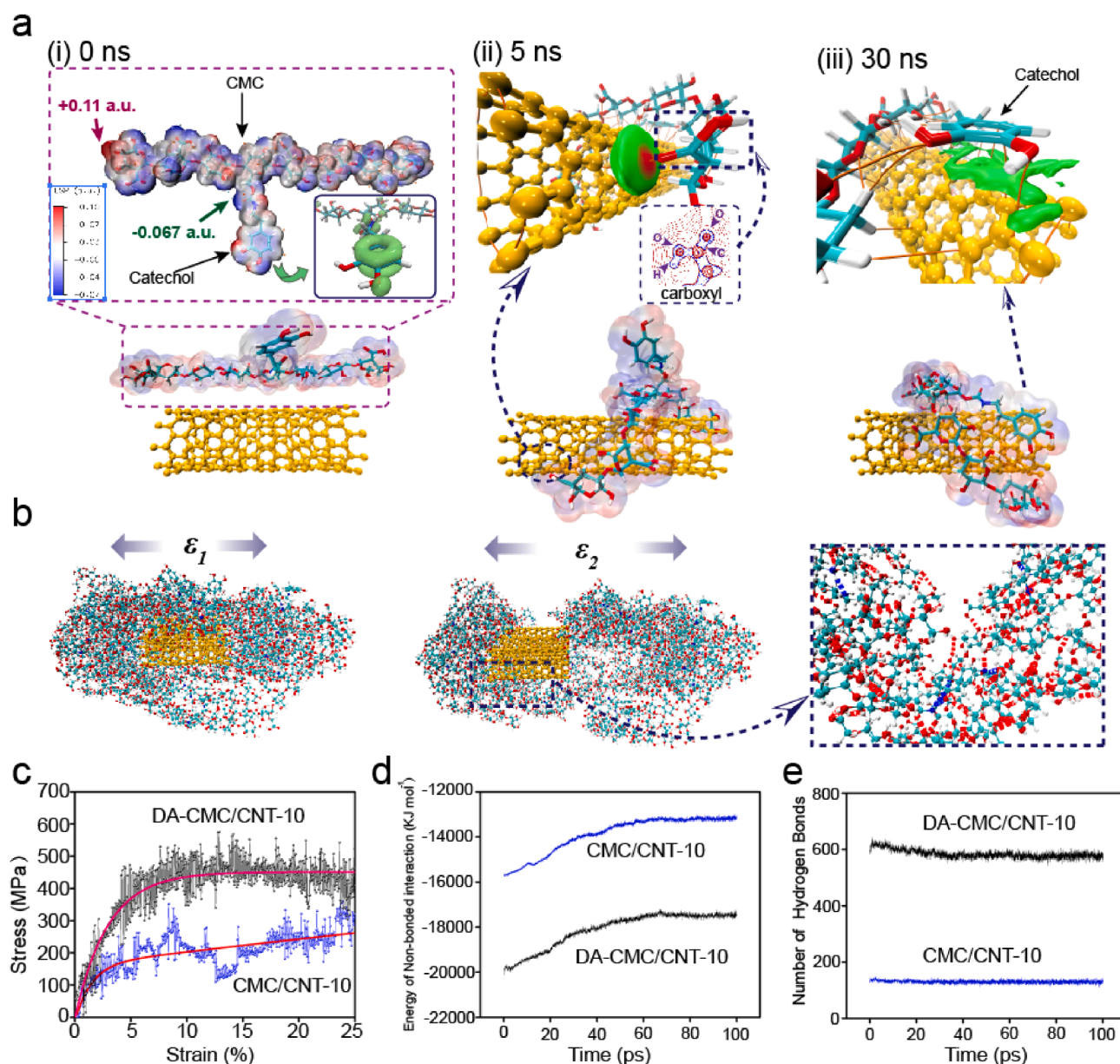


**Fig. 3.** Molecular dynamics simulations of the DA-CMC/CNT composite. (a) The snapshot of the process of DA-CMC wrapping CNT at 0 ns, 5 ns, and 30 ns. (b) SMD-simulated images showing the structural evolution of DA-CMC/CNT. Along the x-axis with increasing strain,  $\epsilon_1 < \epsilon_2$ .  $\epsilon_2$  is the critical strain at which the filament breaks. The simulation were calculated by the gmX tool. (c) Simulated stress-strain curves for CMC/CNT-10 and DA-CMC/CNT filaments. (d) The non-bonded interactions of DA-CMC (also CMC) and CNT, and (e) the number of hydrogen bonds in the system.

To further understand how each component synergistically contribute to the mechanical properties of DA-CMC/CNT, at the microscopic scale, we used molecular dynamics (SMD) simulation of DA-CMC and CNT and investigated the interfacial cohesion and structural stability under different strains of DA-CMC/CNT composites [50]. Before applying strain (Fig. 3b, Video 1), the CNTs were fully embedded in the DA-CMC matrix, which acted as a load-bearing agent and prevented CNTs from interfacial separation. At the onset of straining, the DA-CMC network gradually unfolded. The sequential interfacial interactions in the network structure broke with the increased strain. In the case of the CMC/CNT composites, the interactions between CNT and DA-CMC induced a higher strength than in the absence of DA, which indicates hydrogen bonding formation between the hydroxyl groups (-OH) and the carboxyl groups (-COOH) of CMC, as well as phenolic hydroxyl group (Ar-OH) present in the DA [27]. At a further increased strain, the composite experienced higher normalized stress (Fig. 3c) due to the bridging effect between DA-CMC and CNT, indicating that the DA-CMC/CNT composite was more difficult to fracture than CMC/CNT, at a lower critical strain.

Hydrogen bonding (Fig. 3d) and non-bonded interactions (Fig. 3e) affect CMC and CNT after DA conjugation. Because of the increased

interfacial interactions between CNT and DA-CMC, the composite develops better mechanical strength than that without DA and inhibits CNTs from slipping out from the DA-CMC network. Therefore, at the critical strain, the DA-CMC/CNT composite is more resistant to fracture than CMC/CNT. SMD simulation for stress-strain profiles as a function of DA agree with the experimental data (Fig. 3c). Although the direct evidence for the secondary bonding is difficult to achieve experimentally and would justify a study on its own, further investigation is needed on the interactions between DA-CMC and CNT, for instance by using adhesion measurements via the surface force apparatus or, more conveniently, by using the colloidal probe technique in atomic force microscopy.

### 3.4. Conductivity and stability of DA-CMC/CNT filaments

A wearable sensor was developed from the DA-CMC/CNT filaments and its electroactive was systematically investigated under mechanical stress. Fig. 4a depicts the normalized resistance of CMC/CNT and DA-CMC/CNT filaments as a function of CNT content. The electrical resistance decreased considerably with CNT addition (i.e., the conductivity increased with CNT loading). The DA-CMC/CNT filaments with 5–20%

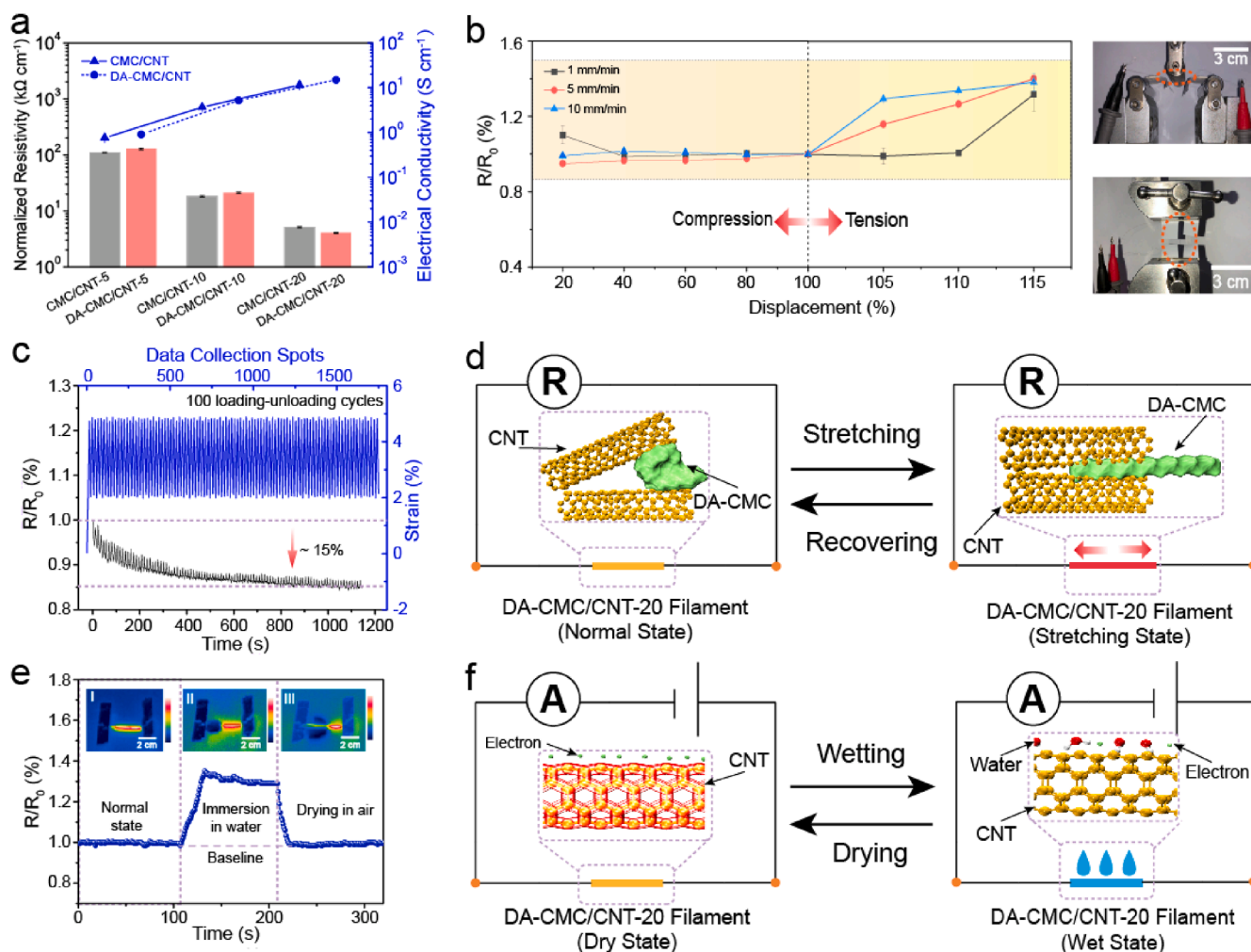


**Fig. 4.** Stability of DA-CMC/CNT filaments under different demands. (a) Volume resistivity ( $R/R_0$ ) (grey and red) and electrical conductivity (blue) versus CNT content in the filaments; (b) Changes in electrical resistance under compression and tensile loading at various deformation rates (1, 5, 10 mm/min). Right: photos taken during testing. (c) Electrical-resistance variation of a DA-CMC/CNT-10 filament undergoing 100 loading/unloading cycles under a strain of 4.8%. (d) Schematics illustration of the mechanism affecting the electrical resistance under elastic deformation. (e) Demonstration of a DA-CMC/CNT filament acting as a sensor in air and in water: relative resistance changes of a sample during immersion-drying (water/air) at 20 °C. Inset: infrared photos following the (i) original, (ii) immersion, and (iii) drying process. (f) Schematics illustration of the mechanism affecting the electrical resistance of the filaments when immersed in water. (For interpretation of the references to colour in this figure legend, the reader is referred to the web version of this article.)

CNT exhibited a volume resistivity between 128.2 and 4.04 k $\Omega$  cm<sup>-1</sup> (i.e., a conductivity of 0.90 to 14.92 S cm<sup>-1</sup>, Table S5). Fig. 4b presents the R/R<sub>0</sub> of a single DA-CMC/CNT filament under compressive and tensile stresses in the longitudinal direction. Notably, the R/R<sub>0</sub> exhibited a quite stable behavior under compressive stress, regardless of the deformation rate. The value of R/R<sub>0</sub> increased monotonically under a tensile stress of 100–115%, owing to the fact that faster deformation rates (5 and 10 mm/min) induced more structural flaws, originated by stress accumulation. The stability of DA-CMC/CNT filaments during use (Figure S11, Video 2), including knotting and bending, demonstrate their suitability and large range of operational strain, making them ideal for deformation sensors.[51]

In order to demonstrate filament performance as a wearable platform, we further analyzed the DA-CMC/CNT structure and its electrical stability by cyclic loading–unloading tests. As shown in Fig. 4c, under a deformation of ~4.8%, the electrical resistance decreases by 15%. After 100 loading–unloading cycles, the tested filaments performed as a wire in the circuit (Figure S12). To explore the influence of tension rate on the conductivity of the composite filaments, we applied a 10 mm/min stretching rate, where the electrical resistance started to increase at first (Figure S13). However, the resistance decreased with the deformation from 6% to 3%, indicating that the recovery of the DA-CMC networks as well as the interfacial bonding between building blocks. In comparison with results at a strain rate of 1 mm/min, the electrical resistance of the filament was increased when a pulling force was applied at a rate of 10 mm/min, which indicates that upon fast deformation (stretching), the building blocks might slip and disassemble the network within the composite filament. Typically, the post-yield modulus decreases either because crack formation or reorientation of the filaments along the test direction [19]. Interestingly, the Young's modulus remained unchanged upon unloading at the post-yield strain. This suggests the absence of structural changes: the otherwise sliding dislocations that occur between molecular chains, responsible for plastic deformation, are replaced by a stick–slip behavior (Fig. 4d) [48]. This is also verified by molecular dynamics simulations (Fig. 3), which indicated that secondary bonding (hydrogen bonding, non-bonded interactions) remained unchanged during filament sliding [32].

The composite filaments displayed suitable mechanical performance in high humidity conditions. To meet the requirements of wearable electronics and to elucidate the stability of the structure, we conducted a test by placing water on the surface of DA-CMC/CNT filaments [52]. Infrared images were obtained during the immersion process (Fig. 4e). Clearly, the R/R<sub>0</sub> increased rapidly and reached a very high value, about 150%, after immersion for 20 s. The results are explained by water adsorption on CNT, donating electrons to the valence band and causing the electrical resistance to increase [53]. The reversible hygroscopic swelling of the DA-CMC matrix disrupted the electron transport between CNT networks and caused the electrical resistance to increase with humidity [54]. This fast and reliable response indicated water-responsive DA-CMC/CNT filaments. A subsequent continuous decrease of R/R<sub>0</sub> was observed before drying, due to the reconstruction of some damaged conductive CNT networks originating from the highly hygroscopic swelling of the DA-CMC matrix [47]. For the drying process, the R/R<sub>0</sub> decreased to values close to the initial level measured in air for 15 s, i.e., the DA-CMC/CNT filaments recovered after exposure to water. This water sensing behavior is the result of the unique structure of DA-CMC that is relevant to wearable electronic sensors, for example, to monitor body sweat or humidity. As shown in Fig. 4f, the electrical resistance of the filaments increased when immersed in deionized water. The CNT generated heat when it was energized. At the same time, the electrical resistance slightly decreased with temperature, due to Joule heating [55]. The immersion-drying process was repeated for several times to confirm the water resistance ability of the filaments, Figure S14.

### 3.5. Sensing performance of DA-CMC/CNT filaments

The conductivity, ductility, and water sensitivity, together with the piezoresistive response characteristics of the DA-CMC/CNT filaments were investigated. The sensors consisted of a yarn obtained by twisting five filaments and adhering two layers of PE tape (Fig. 5a). The DA-CMC/CNT sensors presented a high sensitivity and reliable piezoresistive response to dynamic out-of-plane pressure (applied by using 10, 20, 30, 50, 100 g loads), and also with 13 constant and periodic pressure weights of 10 g (Fig. 5b). The reduction in resistance is linked to structural variations within the filaments, in which the junction points of neighboring CNTs are densified under load. Besides, the interfaces formed between DA-CMC and CNT endured tensile stress loading, creating close contact between the nanotubes, which increased electrical percolation. Such excellent load-bearing capacity enabled the system to sense small changes in mass [56].

To evaluate a real-life application of the DA-CMC/CNT filament-based sensors, they were attached to different body parts of a volunteer (finger, knee, elbow, wrist, gluteus, bicep, trapezius, and deltoid, see details in Figure S15) and used to monitor, in real time, the motions during exercising. As shown in Fig. 5c, during gluteus training, the signal increased rapidly upon hip lifting and completely recovered the original value when returning to the initial position. This demonstrated a fast response and reliability of the sensor device. The bending of a deltoid muscle, at a given angle and intensity, was monitored by measuring the relative variation in resistance (Fig. 5d). The complex bending movement in the joint, including knee and wrist periodic movements, were precisely monitored. The relative resistance waveform signals varied when the joint bending changed under different frequencies, between fast and slow bending (Fig. 5e). The above results demonstrate the durability and reliability of DA-CMC/CNT filament-based sensor placed on a dynamic surface, which show great potential in wearable/flexible electronics and bio-devices, especially for real-time monitoring and for assessing the performance during movement or exercise. The durability and reliability of the composite filaments open the possibility to create conformable wearables. The introduced systems can be expected for use in point-of-care settings to create smart physical assistance and therapeutic wearable devices that are personalized and tailored to the patient's condition and body.

### 3.6. Electrothermal performance of DA-CMC/CNT filaments

Materials comprising CNT are attractive for energy-efficient electrothermal heating, given their extraordinary Joule heating performance [57]; therefore, we developed a hand glove with an integrated wearable heater and a temperature sensor (Fig. 6a, Video 3). The glove can be tailored to the patient's needs in thermotherapy, where application of heat at the point of injury is required during a prolonged time, namely, to enhance blood flow and to reduce pain [58]. Fig. 6b shows the infrared image of the glove used during heat delivery and temperature sensing. In addition, the Joule heating properties of the DA-CMC/CNT filaments were investigated by recording the temperature evolution over time. The electrothermal performance of filaments made into composite yarns, as obtained by twisting single DA-CMC/CNT-20 filament(s) (1, 3, and 5), was analyzed by monitoring their corresponding temperature–time profiles (Fig. 6c). When the number of filament(s) was 1, 3, or 5, the saturation temperature (determined based on the balance between generated and dissipated heat energy) for DA-CMC/CNT-20 yarns was 32.6, 58.4, or 91.7 °C, respectively. The temperature profiles obtained for the woven comprising the given number of DA-CMC/CNT-10 filaments showed a similar variation (Figure S16). The saturation temperature of the composite yarns increased significantly with the number of single filaments. The maximum temperature of the DA-CMC/CNT yarns was higher than that of single composite filament under the same voltage, indicating less heat energy loss within the composite yarn. On the other hand, under a given working voltage (15

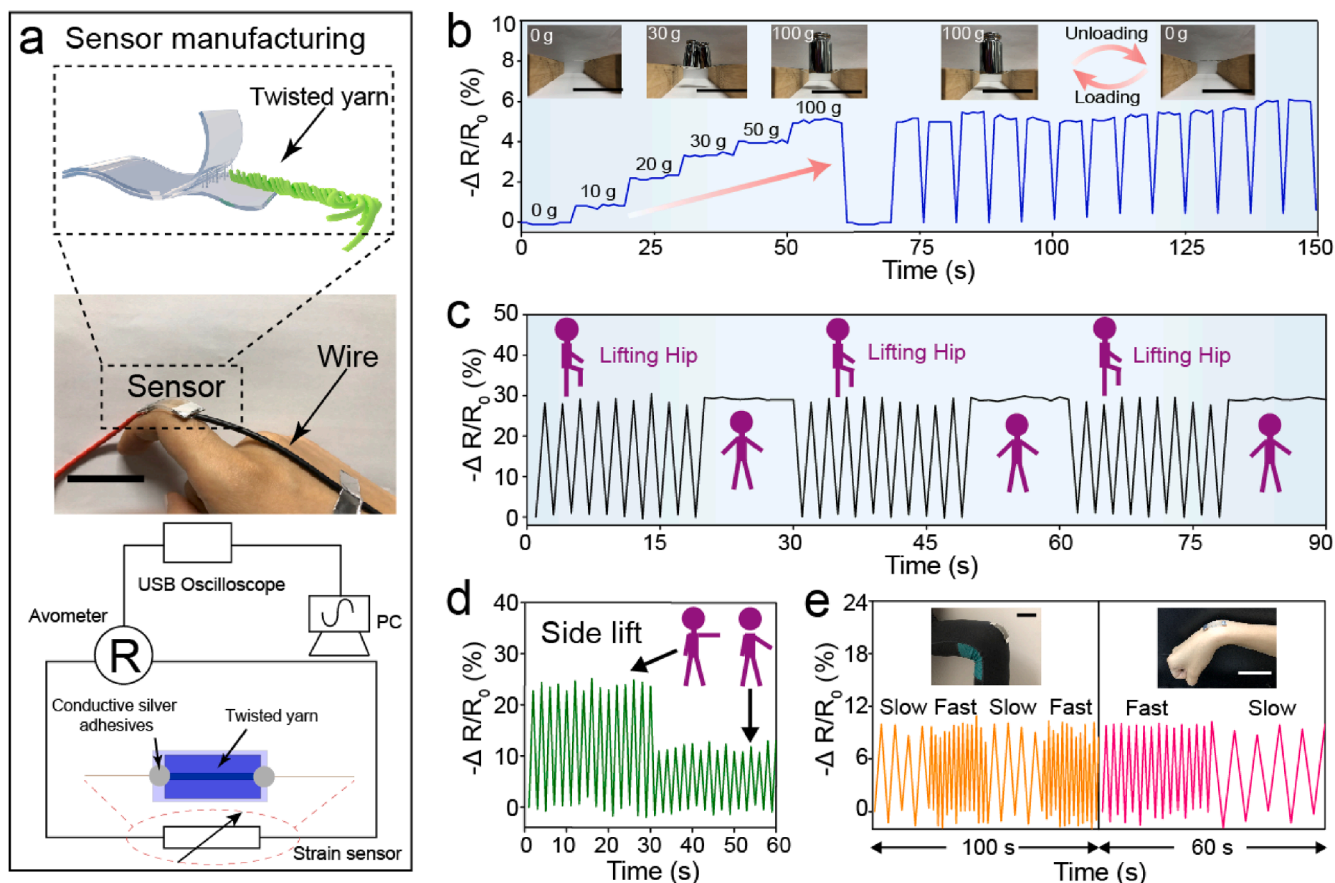


Fig. 5. DA-CMC/CNT filaments as strain sensors. (a) Schematic diagram of the fabrication of a DA-CMC/CNT sensor, and respective photo during finger bending. (b) Piezoresistive response of DA-CMC/CNT filament-based sensor used dynamically for vertical load sensing by increasing weights, and 13 constant and periodic pressure weights of 10 g. Real-time relative resistance variation of the DA-CMC/CNT filament with 10% CNT used as wearable strain sensors for monitoring human movement: (c) gluteus; (d) deltoid; (e) knee and wrist. Notes: the photos in (a, e) were taken with the help of a volunteer.

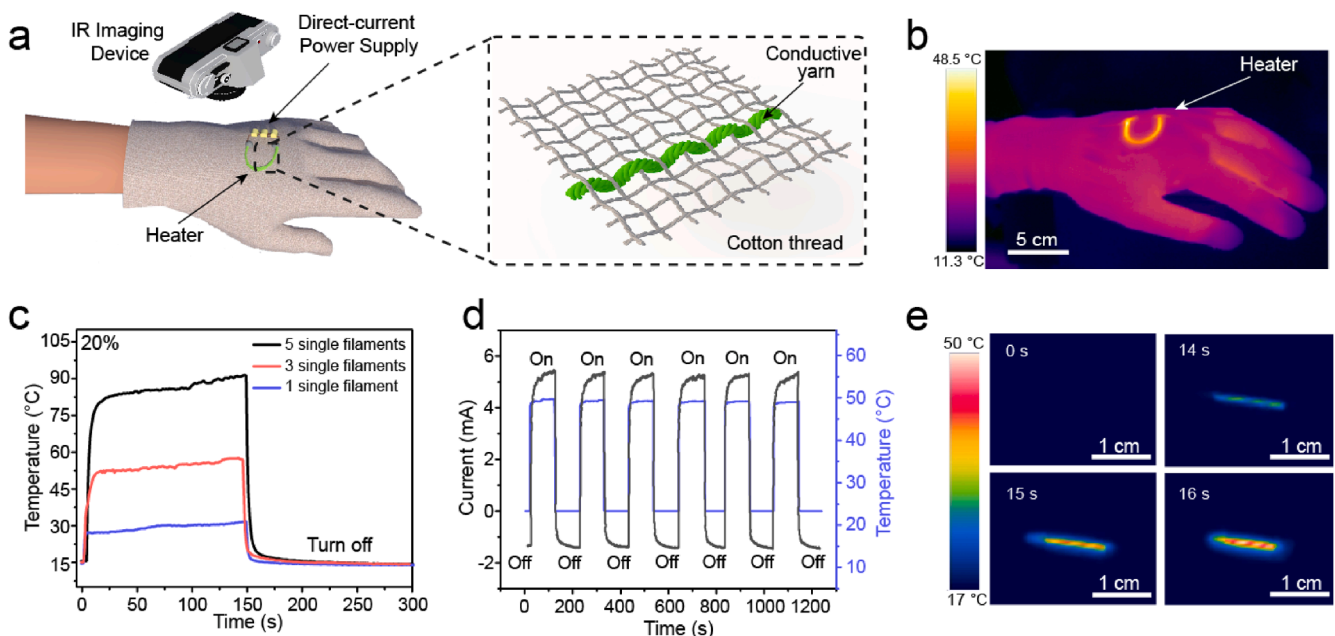


Fig. 6. Electrothermal performance of DA-CMC/CNT filaments/yarns and woven structures. (a) Schematic illustration of a glove that integrates twisted DA-CMC/CNT yarns. (b) Thermography of the glove worn while powered on. (c) Temperature profiles of DA-CMC/CNT-20 woven comprising the given number of filaments under 15 V. Temperature-time and the corresponding current-time curves (d) and thermography images (e) of DA-CMC/CNT-20 filaments with a single filament under a 15 V input voltage for six cycles.

V), the saturated temperature of a single DA-CMC/CNT filament increased with increasing CNT content, which suggests that the composite filaments generated more thermal energy ( $Q = U^2 R^{-1} t^{-1}$ ) at lower electrical resistance.

To further evaluate the electrothermal stability of the DA-CMC/CNT-20 yarns, the cycling temperature variation of a composite woven textile made with a single filament was recorded under 15 V input voltage for approximately 100 s (on) and then naturally cooled to room temperature (off) for six on/off cycles (Fig. 6d). For the cyclic testing, a direct current (DC) voltage was provided by a power supply to both ends of the woven through copper wires and the temperature variation was recorded using a real-time IR thermal imaging camera (Fig. 6e, Video 4). The Joule heating performance of the composite did not show any significant deterioration during the cycling process, further demonstrating excellent electrothermal stability even for a single filament. The fast response of DA-CMC/CNT woven is attributed to their high specific electrical conductivity, while the relatively low mass (5–20% CNT content) of DA-CMC/CNT filament was suitable for heating. The electrical resistance and current of the filament remained stable during six power cycles under 15 V direct voltage. Remarkably, the electrical resistance became easier to stabilize after the sixth cycle, which is attributed to the moisture evaporation from the filaments caused by the rising temperature (Figure S17). The highest input voltage (15 V) used in this work was lower than the standard safe voltage (36 V) of human body, indicating operation as safe and reliable electrical heater. In sum, we demonstrated efficient heating, ultrafast electrothermal response, and good flexibility. Taken all results together, the DA-CMC/CNT filament show promise for its excellent performance in large-area flexible heating.

#### 4. Conclusions

In conclusion, we report on the fabrication of supertough DA-CMC/CNT filaments by exploiting the synergistic effects of hydrogen bonding and non-bonding interactions (including anion- $\pi$ , H- $\pi$ , and  $\pi$ - $\pi$  interactions). The filaments produced by dopamine-conjugated CMC with dispersed CNT exhibited excellent toughness ( $\sim 76.2 \text{ MJ m}^{-3}$ ) and displayed a high failure strain ( $\sim 14.8\%$ ) under high humidity (90% RH). The DA-CMC/CNT filaments supported more than 100 loading-unloading cycles with conductivity retention of about 85%, under different loading levels. Furthermore, the filaments were demonstrated as highly sensitive to water and operated reproducibly. The multifunctional DA-CMC/CNT filaments and ensuing wearables were also demonstrated as sensors for body monitoring and wearable electrothermal heating. The obtained results enable the development of next-generation, low cost bio-based wearable electronic textiles for multiple uses.

#### Declaration of Competing Interest

The authors declare that they have no known competing financial interests or personal relationships that could have appeared to influence the work reported in this paper.

#### Acknowledgements

This work is supported by the National Natural Science Foundation of China (Grant No. 31730106, 31770623, 31670555) and NSERC Canada. O.J.R. acknowledges the Canada Excellence Research Chair initiative and Canada Foundation for Innovation (CFI). T.G. would like to acknowledge the financial support from China Scholarship Council (CSC). We thank technician Dr. Huihua Min in the Advanced Analysis Test Center at Nanjing Forestry University for technical assistance.

#### Appendix A. Supplementary data

Supplementary data to this article can be found online at <https://doi.org/10.1016/j.cej.2021.128981>.

[org/10.1016/j.cej.2021.128981](https://doi.org/10.1016/j.cej.2021.128981).

#### References

- [1] K. Sim, Z. Rao, Z. Zou, F. Ershad, J. Lei, A. Thukral, J. Chen, Q.-A. Huang, J. Xiao, C. Yu, Metal oxide semiconductor nanomembrane-based soft unnoticeable multifunctional electronics for wearable human-machine interfaces, *Sci. Adv.* 5 (2019) eaav9653.
- [2] G.-H. Lee, H. Moon, H. Kim, G.H. Lee, W. Kwon, S. Yoo, D. Myung, S.H. Yun, Z. Bao, S.K. Hahn, Multifunctional materials for implantable and wearable photonic healthcare devices, *Nat. Rev. Mater.* 5 (2) (2020) 149–165, <https://doi.org/10.1038/s41578-019-0167-3>.
- [3] M. Yamawaki, M. Ohnishi, S. Ju, J. Shiomi, Multifunctional structural design of graphene thermoelectrics by Bayesian optimization, *Sci. Adv.* 4 (6) (2018) eaar4192, <https://doi.org/10.1126/sciadv.aar4192>.
- [4] J.A. Lee, Y.T. Kim, G.M. Spinks, D. Suh, X. Lepró, M.D. Lima, R.H. Baughman, S. J. Kim, All-Solid-State Carbon Nanotube Torsional and Tensile Artificial Muscles, *Nano Lett.* 14 (5) (2014) 2664–2669, <https://doi.org/10.1021/nl500526r>.
- [5] P. Chen, Y. Xu, S. He, X. Sun, S. Pan, J. Deng, D. Chen, H. Peng, Hierarchically arranged helical fibre actuators driven by solvents and vapours, *Nature Nanotech* 10 (12) (2015) 1077–1083, <https://doi.org/10.1038/nnano.2015.198>.
- [6] Z. Lu, J. Foroughi, C. Wang, H. Long, G.G. Wallace, Superelastic Hybrid CNT/Graphene Fibers for Wearable Energy Storage, *Adv. Energy Mater.* 8 (8) (2018) 1702047, <https://doi.org/10.1002/aenm.201702047>.
- [7] Y. Li, Y. Li, M. Su, W. Li, Y. Li, H. Li, X. Qian, X. Zhang, F. Li, Y. Song, Electronic Textile by Dyeing Method for Multiresolution Physical Kinetics Monitoring, *Adv. Electron. Mater.* 3 (10) (2017) 1700253, <https://doi.org/10.1002/aem.201700253>.
- [8] L. Dai, Y. Wang, X. Zou, Z. Chen, H. Liu, Y. Ni, Ultrasensitive Physical, Bio, and Chemical Sensors Derived from 1-, 2-, and 3-D Nanocellulosic Materials, *Small* 16 (13) (2020) 1906567, <https://doi.org/10.1002/sml.201906567>.
- [9] S. Lee, S. Shin, S. Lee, J. Seo, J. Lee, S. Son, H.J. Cho, H. Algadi, S. Al-Sayari, D. E. Kim, T. Lee, Ag Nanowire Reinforced Highly Stretchable Conductive Fibers for Wearable Electronics, *Adv. Funct. Mater.* 25 (21) (2015) 3114–3121, <https://doi.org/10.1002/adfm.201500628>.
- [10] R. Zhang, Q. Wen, W. Qian, D.S. Su, Q. Zhang, F. Wei, Superstrong Ultralong Carbon Nanotubes for Mechanical Energy Storage, *Adv. Mater.* 23 (30) (2011) 3387–3391, <https://doi.org/10.1002/adma.201100344>.
- [11] M. Kanik, S. Orguc, G. Varnavides, J. Kim, T. Benavides, D. Gonzalez, T. Akintilo, C.C. Tasan, A.P. Chandrakasan, Y. Fink, P. Anikeeva, Strain-programmable fiber-based artificial muscle, *Science* 365 (2019) 145–150.
- [12] Y. Cheng, R. Wang, K.H. Chan, X. Lu, J. Sun, G.W. Ho, A Biomimetic Conductive Tendril for Ultrapliable and Integratable Electronics, Muscles, and Sensors, *ACS Nano* 12 (4) (2018) 3898–3907, <https://doi.org/10.1021/acsnano.8b01372.s003>.
- [13] J.-G. Kim, S.J. Hong, H. Kang, D. Suh, Anomalous Negative Resistance Phenomena in Twisted Superconducting Nanowire Yarns, *ACS Nano* 14 (3) (2020) 3337–3343, <https://doi.org/10.1021/acsnano.9b09026.s001>.
- [14] T. Cui, S. Mukherjee, P.M. Sudeep, G. Colas, F. Najafi, J. Tam, P.M. Ajayan, C. V. Singh, Y.u. Sun, T. Filleter, Fatigue of graphene, *Nat. Mater.* 19 (4) (2020) 405–411, <https://doi.org/10.1038/s41563-019-0586-y>.
- [15] A. Wei, S. Lahkar, X. Li, S. Li, H. Ye, Multilayer Graphene-Based Thermal Rectifier with Interlayer Gradient Functionalization, *ACS Appl. Mater. Interfaces* 11 (48) (2019) 45180–45188, <https://doi.org/10.1021/acsaami.9b11762.s001>.
- [16] C. Jiang, A. Saha, C.C. Young, D.P. Hashim, C.E. Ramirez, P.M. Ajayan, M. Pasquali, A.A. Martí, Macroscopic Nanotube Fibers Spun from Single-Walled Carbon Nanotube Polyelectrolytes, *ACS Nano* 8 (9) (2014) 9107–9112, <https://doi.org/10.1021/nn502552q>.
- [17] Z. Xu, Y. Liu, X. Zhao, L.i. Peng, H. Sun, Y. Xu, X. Ren, C. Jin, P. Xu, M. Wang, C. Gao, Ultrapliff and Strong Graphene Fibers via Full-Scale Synergetic Defect Engineering, *Adv. Mater.* 28 (30) (2016) 6449–6456, <https://doi.org/10.1002/adma.201506426>.
- [18] Z. Lu, J. Foroughi, C. Wang, H. Long, G.G.J.A.E.M. Wallace, Superelastic hybrid CNT/graphene fibers for wearable energy storage, *Adv. Energy Mat.* 8 (2018) 1702047, <https://doi.org/10.1002/aenm.201702047>.
- [19] N. Mittal, F. Ansari, V.K. Gowda, C. Brouzet, P. Chen, P.T. Larsson, S.V. Roth, F. Lundell, L. Wagberg, N.A. Kotov, L.D. Soderberg, Multiscale Control of Nanocellulose Assembly: Transferring Remarkable Nanoscale Fibril Mechanics to Macroscale Fibers, *ACS Nano* 12 (2018) 6378–6388.
- [20] U.G.K. Wegst, H. Bai, E. Saiz, A.P. Tomsia, R.O. Ritchie, Bioinspired structural materials, *Nat. Mater.* 14 (2014) 23.
- [21] Z. Wan, C. Chen, T. Meng, M. Mojtaba, Y. Teng, Q. Feng, D. Li, Multifunctional Wet-Spun Filaments through Robust Nanocellulose Networks Wrapping to Single-Walled Carbon Nanotubes, *ACS Appl. Mater. Interfaces* 11 (45) (2019) 42808–42817, <https://doi.org/10.1021/acsaami.9b15153.s005>.
- [22] Y. Zhang, J. Peng, M. Li, E. Saiz, S.E. Wolf, Q. Cheng, Bioinspired Supertough Graphene Fiber through Sequential Interfacial Interactions, *ACS Nano* 12 (9) (2018) 8901–8908, <https://doi.org/10.1021/acsnano.8b04322>.
- [23] W. Liu, X. Zhang, G. Wei, Z. Su, Reduced Graphene Oxide-Based Double Network Polymeric Hydrogels for Pressure and Temperature Sensing, *Sensors (Basel)* 18 (2018).
- [24] C. Shao, M. Wang, L. Meng, H. Chang, B.o. Wang, F. Xu, J. Yang, P. Wan, Mussel-Inspired Cellulose Nanocomposite Tough Hydrogels with Synergistic Self-Healing, Adhesive, and Strain-Sensitive Properties, *Chem. Mater.* 30 (9) (2018) 3110–3121, <https://doi.org/10.1021/acs.chemmater.8b01172.s004>.

- [25] X. Lei, D. Ye, J. Chen, S. Tang, P. Sun, L. Chen, A. Lu, Y. Du, L. Zhang, Customizable Multidimensional Self-Wrinkling Structure Constructed via Modulus Gradient in Chitosan Hydrogels, *Chem. Mater.* 31 (24) (2019) 10032–10039, <https://doi.org/10.1021/acs.chemmater.9b02812.s003>.
- [26] D. Zhao, Y. Zhu, W. Cheng, G. Xu, Q. Wang, S. Liu, J. Li, C. Chen, H. Yu, L. Hu, A Dynamic Gel with Reversible and Tunable Topological Networks and Performances, *Matter* 2 (2) (2020) 390–403, <https://doi.org/10.1016/j.matt.2019.10.020>.
- [27] T. Guo, L. Gu, Y.u. Zhang, H. Chen, B.o. Jiang, H. Zhao, Y. Jin, H. Xiao, Bioinspired self-assembled films of carboxymethyl cellulose–dopamine/montmorillonite, *J. Mater. Chem. A* 7 (23) (2019) 14033–14041, <https://doi.org/10.1039/C9TA00998A>.
- [28] J. Zhang, L. Xiang, B. Yan, H. Zeng, Nanomechanics of Anion- $\pi$  Interaction in Aqueous Solution, *J. Am. Chem. Soc.* 142 (2020) 1710–1714.
- [29] H. Kim, G. Kim, Adsorption properties of dopamine derivatives using carbon nanotubes: A first-principles study, *Appl. Surf. Sci.* 501 (2020) 144249, <https://doi.org/10.1016/j.apsusc.2019.144249>.
- [30] M.M. Hamed, A. Hajian, A.B. Fall, K. Håkansson, M. Salajkova, F. Lundell, L. Wågberg, L.A. Berglund, Highly Conducting, Strong Nanocomposites Based on Nanocellulose-Assisted Aqueous Dispersions of Single-Wall Carbon Nanotubes, *ACS Nano* 8 (3) (2014) 2467–2476, <https://doi.org/10.1021/nm4060368>.
- [31] A. Hajian, S.B. Lindström, T. Pettersson, M.M. Hamed, L. Wågberg, Understanding the Dispersive Action of Nanocellulose for Carbon Nanomaterials, *Nano Lett.* 17 (3) (2017) 1439–1447, <https://doi.org/10.1021/acs.nanolett.6b04405.s001>.
- [32] H. Zhu, S. Zhu, Z. Jia, S. Parvinian, Y. Li, O. Vaaland, L. Hu, T. Li, Anomalous scaling law of strength and toughness of cellulose nanopaper, *PNAS* 112 (29) (2015) 8971–8976, <https://doi.org/10.1073/pnas.1502870112>.
- [33] A.G. Ryabenko, T.V. Dorofeeva, G.I. Zvereva, UV–VIS–NIR spectroscopy study of sensitivity of single-wall carbon nanotubes to chemical processing and Van-der-Waals SWNT/SWNT interaction. Verification of the SWNT content measurements by absorption spectroscopy, *Carbon* 42 (8–9) (2004) 1523–1535, <https://doi.org/10.1016/j.carbon.2004.02.005>.
- [34] Y. Nishiyama, Structure and properties of the cellulose microfibril, *J Wood Sci* 55 (4) (2009) 241–249, <https://doi.org/10.1007/s10086-009-1029-1>.
- [35] W.L. Jorgensen, D.S. Maxwell, J. Tirado-Rives, Development and Testing of the OPLS All-Atom Force Field on Conformational Energetics and Properties of Organic Liquids, *J. Am. Chem. Soc.* 118 (45) (1996) 11225–11236, <https://doi.org/10.1021/ja9621760>.
- [36] R. Khan, W. Gorski, C.D. Garcia, Nanomolar Detection of Glutamate at a Biosensor Based on Screen-Printed Electrodes Modified with Carbon Nanotubes, *Electroanalysis* 23 (10) (2011) 2357–2363, <https://doi.org/10.1002/elan.201100348>.
- [37] T.H. Li, C.M. Wang, S.W. Yu, X.Y. Liu, X.H. Li, X.G. Xie, A theoretical study on the gas phase reaction of Au+ with CH<sub>3</sub>F, *Chem. Phys. Lett.* 463 (4–6) (2008) 334–339, <https://doi.org/10.1016/j.cplett.2008.08.073>.
- [38] F. Weigend, R. Ahlrichs, Balanced basis sets of split valence, triple zeta valence and quadruple zeta valence quality for H to Rn: Design and assessment of accuracy, *PCCP* 7 (18) (2005) 3297, <https://doi.org/10.1039/b508541a>.
- [39] T. Yanai, D.P. Tew, N.C. Handy, A new hybrid exchange–correlation functional using the Coulomb-attenuating method (CAM-B3LYP), *Chem. Phys. Lett.* 393 (1–3) (2004) 51–57, <https://doi.org/10.1016/j.cplett.2004.06.011>.
- [40] S. Grimme, C. Bannwarth, P. Shushkov, A Robust and Accurate Tight-Binding Quantum Chemical Method for Structures, Vibrational Frequencies, and Noncovalent Interactions of Large Molecular Systems Parametrized for All spd-Block Elements (Z = 1–86), *J Chem Theory Comput* 13 (2017) 1989–2009.
- [41] B. Vigolo, A. Penicaud, C. Coulon, C. Sauder, R. Pailler, C. Journet, P. Bernier, P. Poulin, Macroscopic fibers and ribbons of oriented carbon nanotubes, *Science* 290 (2000) 1331–1334.
- [42] A.J. Blanch, C.E. Lenehan, J.S. Quinton, Dispersant Effects in the Selective Reaction of Aryl Diazonium Salts with Single-Walled Carbon Nanotubes in Aqueous Solution, *J. Phys. Chem. C* 116 (2) (2012) 1709–1723, <https://doi.org/10.1021/jp208191c>.
- [43] C. Cheng, S. Li, J. Zhao, X. Li, Z. Liu, L. Ma, X. Zhang, S. Sun, C. Zhao, Biomimetic assembly of polydopamine-layer on graphene: Mechanisms, versatile 2D and 3D architectures and pollutant disposal, *Chem. Eng. J.* 228 (2013) 468–481.
- [44] W. Chen, R. Wang, T. Xu, X. Ma, Z. Yao, B.o. Chi, H. Xu, A mussel-inspired poly ( $\gamma$ -glutamic acid) tissue adhesive with high wet strength for wound closure, *J. Mater. Chem. B* 5 (28) (2017) 5668–5678, <https://doi.org/10.1039/C7TB00813A>.
- [45] Y.i. Deng, X. Gao, X.-L. Shi, S. Lu, W. Yang, C. Duan, Z.-G. Chen, Graphene Oxide and Adiponectin-Functionalized Sulfonated Poly(etheretherketone) with Effective Osteogenicity and Remotely Repeatable Photodisinfection, *Chem. Mater.* 32 (5) (2020) 2180–2193, <https://doi.org/10.1021/acs.chemmater.0c00290.s001>.
- [46] D. Klemm, F. Kramer, S. Moritz, T. Lindström, M. Ankerförs, D. Gray, A. Dorris, Nanocelluloses: a new family of nature-based materials, *Angew. Chem. Int. Ed. Engl.* 50 (2011) 5438–5466.
- [47] H. Qi, B. Schulz, T. Vad, J. Liu, E. Mäder, G. Seide, T. Gries, Novel Carbon Nanotube/Cellulose Composite Fibers As Multifunctional Materials, *ACS Appl. Mater. Interfaces* 7 (40) (2015) 22404–22412, <https://doi.org/10.1021/acsami.5b06229>.
- [48] B. Arash, Q. Wang, V.K. Varadan, Mechanical properties of carbon nanotube/polymer composites, *Sci. Rep.* 4 (2014) 6479.
- [49] T. Lu, F. Chen, Bond Order Analysis Based on the Laplacian of Electron Density in Fuzzy Overlap Space, *J. Phys. Chem. A* 117 (14) (2013) 3100–3108, <https://doi.org/10.1021/jp4010345>.
- [50] X. Liang, H. Li, J. Dou, Q.i. Wang, W. He, C. Wang, D. Li, J.-M. Lin, Y. Zhang, Stable and Biocompatible Carbon Nanotube Ink Mediated by Silk Protein for Printed Electronics, *Adv. Mater.* 32 (31) (2020) 2000165, <https://doi.org/10.1002/adma.202000165>.
- [51] N. Zhou, T. Liu, B. Wen, C. Gong, G. Wei, Z. Su, Recent Advances in the Construction of Flexible Sensors for Biomedical Applications, *Biotechnol. J.* 15 (12) (2020) 2000094, <https://doi.org/10.1002/biot.202000094>.
- [52] H. Qi, E. Mäder, J. Liu, Unique water sensors based on carbon nanotube–cellulose composites, *Sens. Actuators, B* 185 (2013) 225–230.
- [53] T. Villmow, S. Pegel, A. John, R. Rentenberger, P. Pötschke, Liquid sensing: smart polymer/CNT composites, *Mater. Today* 14 (2011) 340–345.
- [54] H. Qi, J. Liu, S. Gao, E. Mäder, Multifunctional films composed of carbon nanotubes and cellulose regenerated from alkaline–urea solution, *J. Mater. Chem. A* 1 (6) (2013) 2161–2168, <https://doi.org/10.1039/C2TA00882C>.
- [55] W.-T. Cao, C. Ma, D.-S. Mao, J. Zhang, M.-G. Ma, F. Chen, MXene-Reinforced Cellulose Nanofibril Inks for 3D-Printed Smart Fibres and Textiles, *Adv. Funct. Mater.* 29 (51) (2019) 1905898, <https://doi.org/10.1002/adfm.201905898>.
- [56] F. Cai, C. Yi, S. Liu, Y. Wang, L. Liu, X. Liu, X. Xu, L.i. Wang, Ultrasensitive, passive and wearable sensors for monitoring human muscle motion and physiological signals, *Biosens. Bioelectron.* 77 (2016) 907–913, <https://doi.org/10.1016/j.bios.2015.10.062>.
- [57] Z. Li, Z. Xu, Y. Liu, R. Wang, C. Gao, Multifunctional non-woven fabrics of interfused graphene fibres, *Nat. Commun.* 7 (2016) 13684.
- [58] H. Ota, S. Emaminejad, Y. Gao, A. Zhao, E. Wu, S. Challa, K. Chen, H.M. Fahad, A. K. Jha, D. Kiriya, W. Gao, H. Shiraki, K. Morioka, A.R. Ferguson, K.E. Healy, R. W. Davis, A. Javey, Application of 3D Printing for Smart Objects with Embedded Electronic Sensors and Systems, *Adv. Mater. Technol.* 1 (1) (2016) 1600013, <https://doi.org/10.1002/admt.201600013>.